

ROCK PIGEON CAVE, COLORADO: DEVELOPMENT AND MINERALOGY

Douglas M. Medville¹

Abstract

The late Cretaceous Mancos Shale in western Colorado contains several vadose caves developed entirely within the shale. The largest of these, Rock Pigeon Cave, is over 300 m in length and contains a seasonal stream. The cave, and others like it, is hypothesized to develop as a result of the oxidation of disseminated pyrite in the shale by descending meteoric water with resulting sulfate ions reacting with the carbonate component of the shale to produce gypsum. The gypsum pries apart the shale, increasing its secondary porosity, and allows flowing water to remove shale particles via corrosion. As these particles are removed, they are transported down-gradient to an outlet, allowing continuous openings (cave passages) to develop. Extensive sulfate mineralization is observed within the cave and takes several forms: soft globular deposits on rocks at water level, a white to tan crust on shale surfaces, dry crusts on the passage floor following evaporation of pools, and needle and hair-like extrusions on passage walls. Powder X-ray diffraction (XRD) indicates that these deposits are a mixture of thenardite and blodite with lesser amounts of gypsum, hexahydrate, and konyaite.

Na⁺, Mg²⁺, and SO₄²⁻ ions in the entering stream are the source of the sulfate minerals at stream level and on the wetted slopes above. These come out of solution as the cave stream and pools evaporate with sulfates precipitating as saturation is reached. Fibrous, needle-like sulfates on walls above the wetted zone are a result of crystallization by evaporation: fluids containing sulfate ions are extruded and evaporate at the rock/air interface. Other minerals, e.g., deposits containing goethite and jarosite, are seen on passage walls as reaction products from oxidation of pyrite in the shale.

INTRODUCTION

Cave passages in fissile shales are usually found in settings where stream erosion in solutional caves incises into shale beds within or below limestones or where surface streams remove shale particles, resulting in shelter caves (Palmer, A., 2007). Vadose caves found entirely within shales and containing active stream or streambeds, while rare, have been reported for an area in north-central Wyoming (Medville, D., 2018) and are also found in western Colorado (this paper).

The occurrence of caves in shales is infrequent due to the conditions to be met for cave development to take place:

- Soils above the shale should contain swelling clays that allow dolines to develop, enhancing the movement of meteoric water to the unweathered shale below.
- Pyrite in the shale is required for reaction with surface and ground water, producing sulfate ions in sufficient quantity to react with calcite in the shale, producing gypsum that, in turn, fractures the shale, increasing its porosity and producing openings that water can flow through.
- A gradient is needed for water to move through openings in the shale to an outlet, allowing shale particles to be removed.
- An arid climate where evaporation exceeds precipitation is needed. If the climate is too wet, although pyrite will oxidize and produce sulfate ions, water moving through the shale may keep ionic concentrations too low for gypsum to precipitate and mechanically wedge the shale apart. This will prevent the development of small voids that can subsequently be enlarged via corrosional processes.

These conditions are met in the study area discussed in this paper: an exposure of soil mantled Mancos Shale in western Colorado. The area lies within the U.S. Bureau of Land Management's Gunnison Gorge National Conservation Area and contains sparse vegetation, deeply incised arroyos, and numerous karst-like features including dolines, blind valleys, and cave entrances. Mean annual precipitation is 30 cm (rain equivalent), and mean annual evaporation is 51 cm (U.S. Department of Agriculture, 2018). Mean annual temperature is 10.5 °C.

METHODS

Bulk mineral analysis of cave wall material was conducted using a Pananalytical X'Pert Pro XRD diffractometer for powder XRD analysis. Continuous scans over a 40-minute period were carried out between 6° and 69° 2θ positions with a step size of 0.017°. Counting peaks provided a semi-quantitative measure of the quantities of mineral components in the samples with peak intensities used to determine the relative proportions of minerals.

Scanning electron microscopy was conducted using a TESCAN-VEGA-3 Integrated Mineral Analyzer (TIMA) coupled with four PulseTor silicon drift EDX detectors for elemental analysis of shale and sulfate minerals at 50 μm-100 μm scales. X-ray counting peaks were consistent with those seen in XRD diffractograms for minerals of interest: primarily

¹ 10701 Pinewalk Way, Highlands Ranch CO 80130, medville@centurylink.net

gypsum, thenardite, and blodite. Stable sulfur isotope measurements were conducted at the University of Waterloo Environmental Isotope Laboratory using a Costech Instruments Elemental Analyzer (CHNS-O ECS 4010) coupled to an Isochrom Continuous Flow Stable Isotope Ratio Mass spectrom. $\delta^{34}\text{S}$ results with respect to the Canyon Diablo Troilite meteorite standard were reported in per mil (‰) units. Temperature and humidity readings in the caves were measured using a Protmex model 6508 digital temperature humidity m accurate to 0.1 °C and 0.1 % RH. A Hanna Instruments model HI98100 m was used to measure cave and surface water pH.

Water samples were collected in pre-washed 250 ml polyethylene bottles that were filled underwater until no air remained. The bottles were placed in containers cooled to 10 °C (cave water temperature) until they were mailed to testing laboratories, usually between 24 and 48 hours after collection. For the samples collected, National Environmental Methods Index Standard Methods (SM) were followed: SM4500 H B for pH; SM 2320 for carbonate, bicarbonate, and alkalinity (as CaCO_3); SM 3120 for Ca, Mg, K, S, Cl, and Fe; and SM 4500 Cl E for Chloride. EPA 353.2 was used for nitrate. These parameters were used as inputs to PHREEQC (Parkhurst, D.L. and C.A. J. Appelo, 1999); the USGS hydrogeochemical modeling software for calculating ion activities and saturation indexes with respect to the various minerals in the water samples taken. Soil compositional analysis was carried out at the Colorado State University Soil, Water, and Plant Testing Laboratory using Inductively Coupled Plasma Optical Emission Spectrometry (Perkin-Elmer Optima 7300V). Methods used to calculate soil pH, alkalinity, sulfates, cations, and Sodium Adsorption Ratio are described in Miller, R.O. et. al., 2013.

RESULTS AND DISCUSSION

Geologic Setting

The late Cretaceous Mancos Shale outcrops over a 1600 km² area between Grand Junction and Montrose, Colorado. The regional outcrop of the Mancos and the study area are shown in Figure 1. The study area is in the upper part of a tributary to Loutsenhizer Arroyo, itself a tributary to the Uncomphagre River, 10 km to the north-west. The area is 0.6 km northeast of the axis of the northward plunging Montrose Syncline. Local dip is about 2 degrees to the southwest.

The Mancos Shale reaches a maximum thickness of nearly 600 m (Hansen, W. R., 1971) and generally consists of calcareous silts with minor limestone, marlstone, bentonite, concretions, and sandstone beds. These rocks represent muddy shelf deposits, and typically

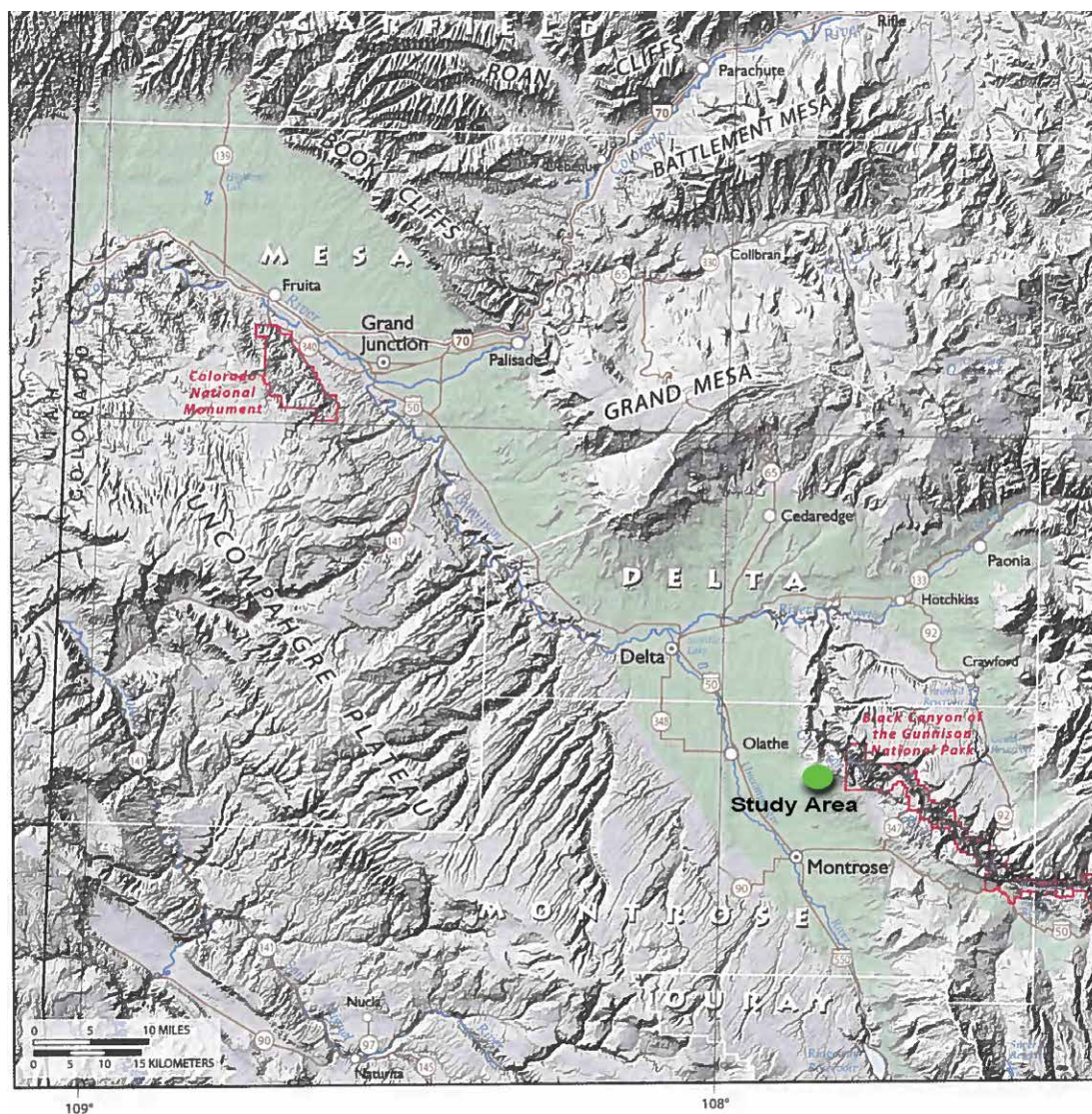


Figure 1. Study area location, Mancos Shale outcrop shown in green. (Source: White, J.L. and C. Greenman, 2008)

form badland-style topography. The local topography is developed on the Niobrara member of the Mancos: a dark gray calcareous shale with a thickness of 230 m to 250 m. The upper Mancos weathers to a pale yellowish-orange or brown color, defined as those portions of Mancos that have undergone significant changes related to weathering processes, chiefly pyrite oxidation to iron hydroxide minerals (Kellogg, K. et. al., 2004; Noe et. al., 2007; U.S. Department of Energy, 2011; White, J.L. et.al., 2014; Noe, D.C., et. al., 2015).

Mancos soils in the study area consist of Wisconsinian age terrace and pediment deposits, primarily a sandy silt. The soils contain soluble Ca^{2+} , Mg^{2+} , Na^+ , and K^+ , as well as gypsum and hydrated Na and Mg sulfates (Whittig, et. al., 1982, Evangelou, et. al., 1984).

The average composition by volume of Mancos soils is 35% clay, 55% silt and 10% sand (Tuttle, M.L., et. al., 2014). The soils mantle the shale beneath and consist of barren or nearly barren outcroppings of gypsiferous and saline shale and some soil material (U.S. Department of Agriculture, 1967). Clays in the Mancos soils are a combination of illite, kaolinite, and up to 15cm thick lenses of montmorillonite, a smectite-group sodium phyllosilicate clay that swells when wetted and desiccates when dried.

The montmorillonite component of the Mancos soils results in a pebbly, adobe-like appearance with shallow desiccation cracks and 2-3 m deep soil dolines in gullies, overlying and aligned with cave passages below (Fig. 2). The soil dolines allow meteoric water to penetrate the regolith, ultimately reaching the unweathered shale below where pyrite oxidation can take place.

Two to three m beneath the local regolith, the weathered Mancos transitions to a darker gray to black unweathered shale where the larger Mancos caves are found. The mean unweathered shale composition based on XRD of nine wall samples taken in six caves in the Mancos is 33 % quartz, 29 % muscovite, and 18 % calcite. The remaining 20 % consists of dolomite, gypsum, and several clays.

Cave Development

The Mancos Shale was deposited in a deep water, anoxic environment and contains significant quantities of disseminated framboidal pyrite. Pyrite oxidation in the weathered zone of the shale creates sulfuric acid that reacts with available calcite in the shale to form gypsum. The gypsum crystallizes along bedding planes in the shale, wedging and

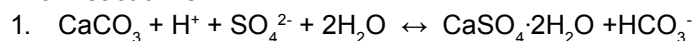


Figure 2. Aligned dolines on Mancos soils.

prying it apart (White, J.L. and C. Greenman, 2008). Also, microfracturing in the shale allows an increase in oxygen influx, accelerating the chemical weathering of both pyrite and carbonate in the shale and increasing its secondary porosity (Gu, X. et.al., 2020). Subsequent dissolution of the gypsum and disaggregation of shale particles via granular removal by meteoric water (i.e., corrasion) result in the development of small subsurface voids. As surface water flows through voids in the fractured shale, micron-scale transportable particles are moved down-gradient to outlets that allow the water to emerge on the surface, carrying with it clay particles from the decomposed shale. Over time, initial voids coalesce and enlarge, allowing humanly enterable passages to develop. Headward erosion (i.e., sapping of the shale) at the down-gradient end of the initial conduit can also result in passage enlargement.

Although the processes differ, the resulting voids can have the same general morphology as caves found in carbonate rock: sinuous, vadose canyon-like passages that under-drain small valleys and contain seasonally flowing water. This process has been observed in the Cretaceous Cody Shale in the Bighorn Basin in north-central Wyoming (Medville, D., 2018) and in the Mancos Shale in western Colorado as described in this paper.

The upper Mancos contains about 1% pyrite (U. S. Department of Energy, 2011). Sulfate ions resulting from pyrite oxidation react with calcium derived from carbonates in the shale to produce gypsum under evaporative conditions. A common reaction is:



The source of the H^+ can be mildly acidic meteoric water (H_2CO_3), which disassociates to H^+ and HCO_3^- ions. The H^+ reacts with the CO_3^{2-} in the calcite to yield Ca^{2+} and bicarbonate ions:

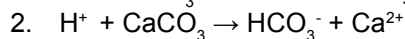
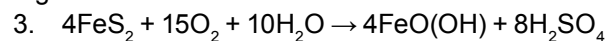


Figure 3. Orange Goethite-containing deposit on passage wall.

The Ca^{2+} reacts with SO_4^{2-} to produce gypsum per reaction (1). Discussions of pyrite oxidation, expansion of pyritic shales, and formation of gypsum are discussed in several reports and papers, e.g., Palmer, A., 2007, Penner, E. et. al., 1972, Nordstrom, D. K., 1982.

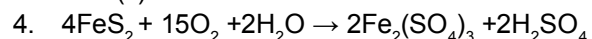
With twice the molar volume of calcite², gypsum is precipitated on shale surfaces in both starburst and fibrous forms. Reaction-induced swelling resulting from gypsum emplacement can lead to microfracturing of the shale, increasing its secondary porosity and enabling surface water to move through it and remove particles via corrasion (Gu et. al., 2020). Dissolution of gypsum interbeds on cave passage walls will also increase secondary porosity, further increasing the occurrence of open spaces between shale beds.

Pyrite in the shale is oxidized by a combination of meteoric water and atmospheric oxygen. Iron in the pyrite precipitates as goethite, an oxyhydroxide seen on cave passage walls and illustrated in Figure 3.



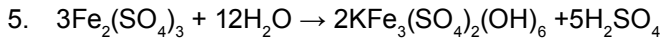
Reaction (3) is a summary of several intermediate reactions involving microbially catalyzed oxidation of ferric sulfides to ferrous and then ferric sulfates, then ferric hydroxide and then dehydration to $\text{FeO}(\text{OH})$. Details are provided in (Penner, E., et. al., 1972; Nordstrom, D.K., 1982, Medville, D., 2018).

Iron can also precipitate as ferric sulfate as per reaction (4).



If potassium is available from the illite clay component in the shale, ferric sulfate can convert to jarosite as per reaction (5).

² Volume change from calcite to gypsum is 2.01. Molar mass gypsum/density gypsum = 172.17 g/mol / 2.32 g/cc = 74.21 cc/mol gypsum. Molar mass calcite/density calcite = 100.09 g/mol / 2.71 g/cc = 36.92 cc/mol calcite. 74.21/36.92 = 2.01.



In the cave studied (Rock Pigeon Cave), samples were taken of gypsum crystals on shale near the upper entrance. These samples had $\delta^{34}\text{S}$ values of -22.03‰ and -19.19‰ , respectively; consistent with the results of a previous study (Tuttle, M.L. et. al., 2014) where the average $\delta^{34}\text{S}$ values from microscopic pyrite in the Mancos Shale was -20‰ . That study concluded that the source of gypsum formation during incipient weathering of the Mancos Shale was from calcite dissolution as a result of acid produced during pyrite oxidation.

The light $\delta^{34}\text{S}$ values are taken as evidence for microbial sulfur isotope fractionation of Cretaceous sulfates when they were reduced to sulfides (FeS_2), which, when oxidized following lowering of the water table, produced sulfate ions that are also light in ^{34}S , as seen in the gypsum samples taken in this study and in the pyrite samples taken in an earlier study (Medville, D., 2018).

Although the Mancos Shale is calcareous, its calcite component does not contribute to cave development as a result of dissolution. The mean calcite content for shale samples taken from the walls of five Mancos caves was 17 %, consistent with a previous study (U.S. Department of Energy, 2011) where a 20 % mean calcite content for Mancos samples was obtained.

While dissolution of the carbonate component of the shale contributes indirectly to passage enlargement via conversion to gypsum, it is not the primary factor in cave development. If, as is the case with the Mancos Shale, the rock is mainly insoluble, dissolution is limited to removing soluble grains from a continuous matrix of insoluble material and is slowed if the insoluble content is more than about 20-30% (Palmer, A., 2007).

The insoluble content of the upper members of the Mancos is about 80 %, consisting of clays, quartz, and muscovite. With contact between aggressive water and calcite grains inhibited by the presence of insoluble material, dissolution is limited. To date, there is no observational evidence of carbonate dissolution in the caves, e.g., rounded, smooth rock surfaces, solution scallops on passage walls, secondary deposition of calcite.

Rock Pigeon Cave

Of the 12 known caves in the Mancos that reach shale bedrock, Rock Pigeon Cave, with 322 m in length and passage up to 15 m in height, is the largest known to date. A map of the cave showing locations where samples were taken for XRD is shown in Figure 4. XRD results are given in Table 1.

The cave is in the Niobrara member of the Mancos, described as a dark-gray to light-gray, calcareous to very calcareous, fissile to sub-platy shale with freshly exposed bedding planes speckled with small white forams and coccoliths (Noe, D.C., et. al., 2015). When viewed under SEM, shale samples taken at the cave's upper entrance show both fram-boidal pyrite and coccoliths, consistent with the description of this member.

The cave's upper entrance (Fig. 5) is developed at the distal end of a 15 m-deep gully; an in feeder to the 30 m-deep northern branch of Loutsenhizer Arroyo.

The unnamed gully in which the cave is found drains an area of 1.8 square km. The entrance is a 7 m-high canyon-like opening 10 m below the local surface.

The cave consists of a single passage that meanders beneath the gully above. Joint-controlled passage orientation is not evident in the cave. The passage has a uniform gradient of 2.6° , the same as that of the 0.67 km long arroyo that carries the stream that flows through the cave

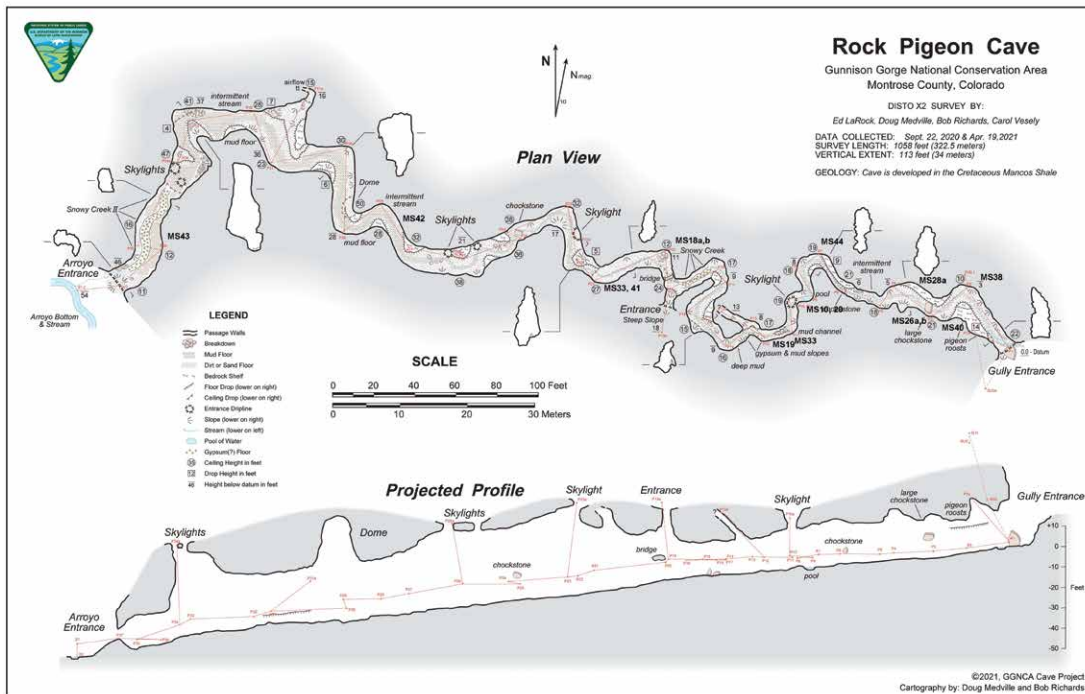


Figure 4. Map of Rock Pigeon Cave with XRD sampling locations.



Figure 5. Upper Rock Pigeon Cave entrance with abandoned drainage above.



Figure 6. Representative passages in Rock Pigeon Cave.

(measured discharge = 0.03 cms). The stream flows for most of the year; drying up between mid-August and mid-October.

The source of the stream is primarily small seeps along the gully with a minor contribution from meteoric water. The cave stream emerges at the cave's lower entrance in a branch of Loutsenhizer Arroyo.

Throughout the cave, the average passage height is 7 m and where seen, consists of a flat horizontal surface in the shale with no apparent change in lithology. The passage floor consists of shale-derived particles forming mud flats containing a shallow

braided stream channel. Slopes of damp and disaggregating shale along and below vertical passage walls are seen through much of the cave. A Photograph of representative cave passage is shown in Figure 6.

The cave has the appearance of a beheaded remnant of a formerly longer cave that would have originated some distance up-gully from the current upper entrance, perhaps at an elevation accordant with the elevation of the current paleo-gully floor above the cave. At present, cave evolution and physical enlargement appear to be actively continuing with wall and ceiling spalling taking place.

With an absence of organic material and speleothems in the cave that can be dated, quantitative methods; e.g. $^{230}\text{Th}/^{234}\text{U}$ decay and carbon-14 dating, are not applicable. A minimum age, however, can be estimated using passage dimensions and local/regional stream and river incision rates. In a series of rainfall-runoff simulations carried out by USGS (Elliott, J.G. et. al., 2007), an incision rate of 0.5 mm/year for gully slopes in excess of 20° was estimated. The simulations were carried out in several small plots 3.4 km SE of the cave in gullies similar to the one containing Rock Pigeon Cave. This incision rate is equivalent to a mass loss of $700 \text{ g m}^{-2} \text{ a}^{-1}$ (Tuttle, M. L. et. al., 2014). The cave's lower entrance, at grade with the branch of Loutsenhizer Arroyo into which it drains, is 3.3 m high. If the initial discharge into the arroyo floor was at current ceiling elevation, an age estimate of $3300 \text{ mm} / 0.5 \text{ mm per year} = 6,600$ years is obtained. This is a minimum estimate that places the cave's origin in a periglacial, post-Pleistocene environment.

Water Chemistry

Two water samples were taken in April 2021: one from the gully stream entering the cave 100 m above the cave's upper entrance and another inside the cave, 200 m below the upper entrance. As expected, water chemistry for both samples were similar: pH was 8.1 and 8.3, conductivity was 18400 and 18970 $\mu\text{mhos cm}^{-1}$, and total dissolved solids were 12270 and 12430 mg L^{-1} , respectively.

Both samples were high in sulfates (6600-7350 mg L^{-1}) and sodium (3900- 4400 mg L^{-1}) with lesser concentrations of Mg (336-426 mg L^{-1}) and calcium (169-205 mg L^{-1}). These and other parameters were entered into PHREEQC. Modeling results indicated that the cave pool water was slightly supersaturated with respect to calcite (SI = +0.49) where SI is the log Saturation Index = log ion activity product - log solubility product. The water was undersaturated with respect to gypsum (SI = -0.3) and halite (SI=-4.86). Surface water results were similar: for CaCO_3 , the SI was +1.86, for gypsum, it was -0.5, and for halite, it was -5.06. Neither thenardite nor blodite SIs were reported for the samples. This was not unexpected: a stream was flowing through the cave, pools were not evaporating, and sulfate evaporites were not being deposited. Since subaqueous deposits were observed under unusually dry conditions when only isolated pools were present, the extent to which the concentration of various species increase as a function of pool evaporation remains to be determined.

Estimates of the relationship between degree of evaporation and ion concentration have been obtained in previous studies. In a study carried out by the USGS in Elephant Skin Wash, 4 km east of the cave, the evaporation of surface water was simulated using PHREEQC (Tuttle, M. L. et. al., 2014). In the simulated evaporation of one liter of solution from a surface pond, blodite did not precipitate (1.5 grams) until 99.98 % of the solution evaporated and mirabilite only precipitated (also 1.5 grams) when 99.3 % of the solution evaporated.

SI as a function of evaporation was also simulated in a study of the evaporation of brines in shallow playas in Spain (Cabestero, O., et. al., 2018). In that study, PHREEQC was used to simulate the increase in brine concentration as evaporation increased. SIs for blodite and thenardite were negative until 84 % of the brine was evaporated. In actual samples taken in the playa, SIs remained negative even as blodite, thenardite, and other species were observed to precipitate.

In Rock Pigeon Cave, PHREEQC was used to simulate the evaporation of pool water. Results were consistent with those of the previous studies in that all species remained in solution even as the simulated pool water evaporation approached 100 % (Fig. 7).

Precipitation of Sulfate Minerals

Mancos soils contain 0.3 % wt gypsum-equivalent salts, of which 0.2 % wt are extractable; primarily calcite, gypsum, Na_2SO_4 , and NaCl (Tuttle, M.L. et. al., 2014). Weathering of the soil (pedogenesis) is marked by a significant decrease in bulk density and an increase in porosity as the shale disaggregates. The porosity increase enables water to move through the soil and redistribute dissolved sulfate ions derived from in situ weathering (Merkler, D., et. al., 2006).

On average, 90 % of precipitation in the immediate area infiltrates the soil, carrying with it salts dissolved at the surface (Elliott, J.G., et. al., 2007). As evaporation takes place, efflorescent sulfate crusts form on the surface of the soil. These may consist of sulfate evaporite species including gypsum ($\text{CaSO}_4 \cdot 2\text{H}_2\text{O}$), thenardite (Na_2SO_4), mirabilite ($\text{Na}_2\text{SO}_4 \cdot 10\text{H}_2\text{O}$), glauberite $\text{Na}_2\text{Ca}(\text{SO}_4)_2$, and blodite ($\text{Na}_2\text{Mg}(\text{SO}_4)_2 \cdot 4\text{H}_2\text{O}$). Soluble salt cations, e.g., Ca^{2+} , Na^+ , Mg^{2+} , K^+ , and anions, e.g., SO_4^{2-} diffuse into solution and are carried into the cave by the entering stream. As a result of evaporation, these solutions can become supersaturated with respect to one or more ions with resulting sulfate precipitation (Onac, B. and P. Forti, 2011).

In Tausoare Cave in Romania, crystallogenesis of sulfate minerals is hypothesized to occur as a result of flooding events where sulfate-enriched water in the cave stream imbue the sediments with the sulfate anion (Onac, B.P., et. al., 2001). This process also applies to Rock Pigeon Cave where, as the stream and pools evaporate, ionic concentrations increase until sulfates are deposited on surfaces including the water/rock interface at pool level, at the high water line through most of the cave, on the passage floor as crusts, and possibly subaqueously.

In Rock Pigeon Cave, both calcium and sodium minerals are observed. Gypsum occurs as 5-10 mm wide starburst crystals on dry rock surfaces and as fibrous fillings between shale beds. Sodium sulfates detected via powder XRD include (a) thenardite, the dehydration product of mirabilite, (b) the hydrated sodium-magnesium salt blodite, (c) hexahydrate ($\text{MgSO}_4 \cdot 6\text{H}_2\text{O}$), and (d) the uncommon hydrated double salt konyaite ($\text{Na}_2\text{Mg}(\text{SO}_4)_2 \cdot 5\text{H}_2\text{O}$), found in evaporated cave water. These sulfates are evident throughout the length of the cave. They are both exogenous, i.e., derived from water entering the cave and endogenous, i.e., from in situ pyrite oxidation taking place within the shale walls of the cave. The sulfates take several forms:

A. Globular precipitates

Soft globular clusters 7-12 mm in diameter are seen at the margins of the cave stream and in evaporating pools. The sulfates are the result of increased ionic concentration as pools evaporate with subsequent crystallization of the observed

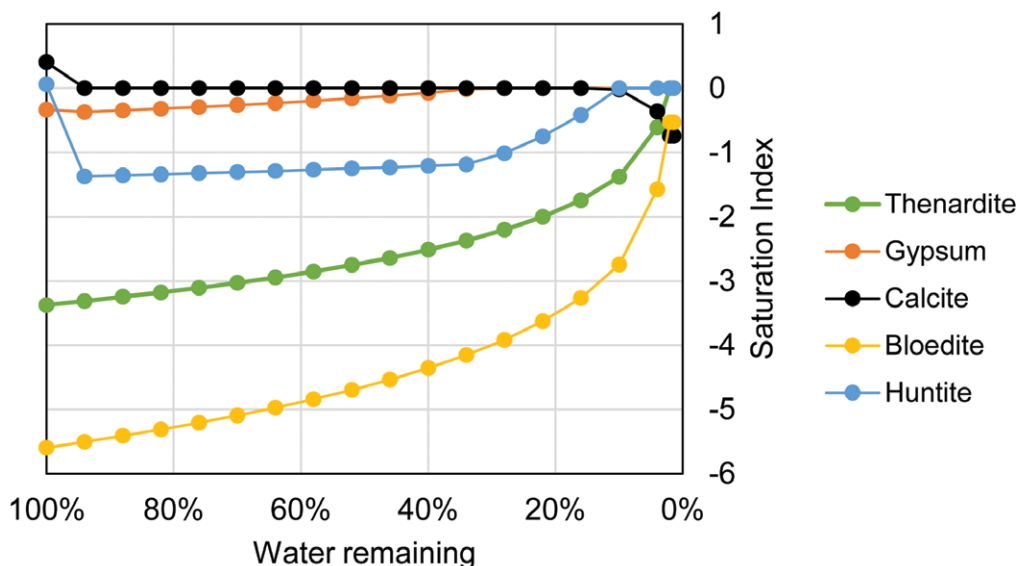


Figure 7: Simulation of evaporating cave water using PHREEQ.

been found to appear seasonally in Tausoare Cave in Romania as environmental conditions in that cave seasonally changed (Onac et. al., 2001) as is observed in Rock Pigeon Cave.

Five samples of the sulfate deposits found at water level were taken at 50 m intervals through the cave. The principal constituents of the crust are thenardite ($\mu = 54.2\%$) and blodite ($\mu = 38.0\%$). Three of the samples contained

minerals. They present as white to yellow/tan precipitates without a nucleation core and are typically roughly rounded cruciform shaped assemblages up to three cm in diam (Figs. 8 and 9).

When placed in distilled water, the clusters dissolve within 15-20 minutes with no insoluble residue remaining, i.e., there does not appear to be any nucleation around a central insoluble core. These evaporites are only found at and immediately above the cave stream and pools. Similar sulfate speleothems have



Figure 8. Globular thenardite/blodite precipitates, 2-3 cm diam.



Figure 9. Globular precipitates at cave stream water level.

Table 1. Rock Pigeon Cave XRD results.

Sample	Description	Percentage												
		muscovite	quartz	kaolinite	calcite	dolomite	gypsum	jarosite	goethite	illite	thenardite	blodite	halite	hexahydrite
MS10	Red wall material	...	26	13	49	8	4
MS18a	Damp shale on floor	21	49	8	11	11
MS18b	Sulfate globules	53	47
MS19	Red wall material	49	31	13	...	7
MS20	Red wall material	35	28	28	5	4
MS23	Dry shale	30	43	8	4	9	6
MS26a	Dry shale above sulfates	...	42	34	5	7	12
MS26b	Damp shale below sulfates	...	46	12	2	9	31	10	9
MS28a	Wall sulfate at high water line	...	28	10	2	4	8	23	16
MS33	Wall needles, filaments	...	9	11	1	4	16	5	18	2
MS37	Twig coatings above cave
MS38	Crystals on dry shale at entrance	...	9	91
MS40	Sulfate globules	5	38	...	8	...
MS41	Sulfate globules	6	25	...	12	...
MS42	Sulfate globules	52
MS43	Sulfate globules	4	28	...	6	...
MS44	Wall needles, filaments	...	36	4	8	9
MS45	Crust from evaporated cave water	36	10	54

gypsum ($\mu=5\%$) and also hexahydrite ($\mu = 8.7\%$). A representative diffractogram for one of the samples (sample MS 18b in Table 1) is shown in Figure 10.

When viewed under SEM, the blodite appears as euhedral tabular crystals (Fig. 11). The accompanying EDX spectrum is consistent with expected energy peaks for blodite. Thenardite is also visible in SEM images, both as bipyramidal and needle shaped forms (Fig. 12).

None of the samples contained the hydrated sulfate mirabilite. To determine whether mirabilite is stable under the temperature and RH conditions in the cave, 15 temperature and relative humidity readings were taken throughout the cave. Air temperature varied from 16.5 °C to 18.6 °C (mean= 17 °C) and RH varied from 45 % to 57 % (mean = 48 %). Figure 179(B) in Hill and Forti (1997) plots the stability of mirabilite and thenardite as a function of temperature and RH. This figure is reproduced in Figure 13 with a data point added for the mean observed conditions in Rock Pigeon Cave (blue square) where in that cave environment, thenardite, but not mirabilite, was found to be stable.

B. Subaqueous white deposits

Subaqueous deposits have been observed in the seasonal evaporation of saline lakes in Spain, Turkey, and elsewhere (del Buey et al., 2021; Cabestrero, O. et al., 2018; Mees, F. et al., 2011; Sonmez, I., 2010; Mutlu, H. et al., 1999; Sonnenfeld, P., 2003). These papers describe conditions under which sulfate minerals, e.g., blodite, thenardite, epsomite, mirabilite, and gypsum nucleate subaqueously as brines in saline and hypersaline lakes evaporate. Similar deposits have been observed in Rock Pigeon Cave where, in isolated evaporating pools, rounded, cruciform shaped white material has been observed both above and below pool level (Fig. 14). In this figure, the subaqueous parts of these deposits are seen where the color changes from white to gray.

Although the appearance of this material is the same as the globular precipitates seen just above water level, as illustrated in Figures 8 and 9, it was only observed once, in September, 2020, during a drought and when no surface water entered the cave and isolated pools in the cave were evaporating. Although observed, samples under these conditions were not taken.

Sulfate minerals that nucleate subaqueously in evaporating playas occur in brines having salinities of 160 to 340 g L⁻¹ (Cabestrero, O. et al., 2018). However, the salinity of pool water samples taken in Rock Pigeon Cave, measured when water was flowing through the cave, was only 4 g L⁻¹. Pool water salinity under evaporative conditions when the sub-

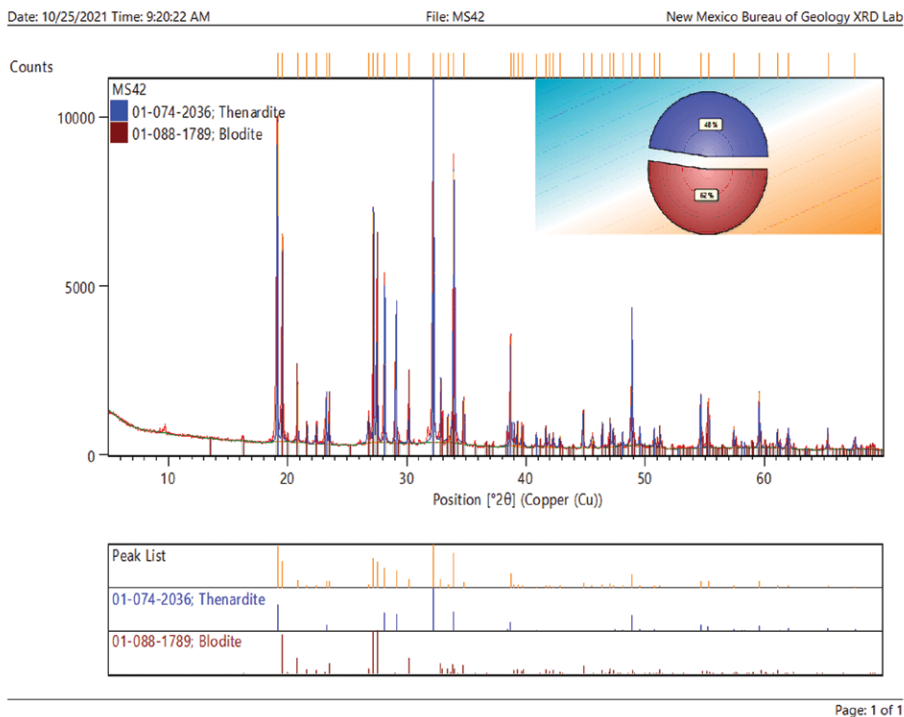


Figure 10. Diffractogram for water-level globular precipitates (sample MS42).

The sulfate component of the crusts is interpreted as being the result of deposition following evaporation of water in the cave stream and pools at and below the top of shale slopes.

aqueous deposits exist has not been measured since these conditions were only seen once, during drought.

C. Coatings on shale

A prominent 3-5 mm thick coating on damp, partially decomposed shale slopes along passage walls is observed through much of the cave. Figure 15 shows this coating, up to a m above stream level and extending from stream level to a point where the disaggregating shale slope meets the dry vertical passage wall above. This may represent a high water mark for the cave stream. Figure 16 is a representative sample of the material, showing a partial crust. The composition of the crusts: half sulfates and carbonates, half quartz and clays, is a result of the difficulty of separating the sulfates from the underlying shale on which they are deposited. The composition of this material (sample MS28a) is listed in Table 1.

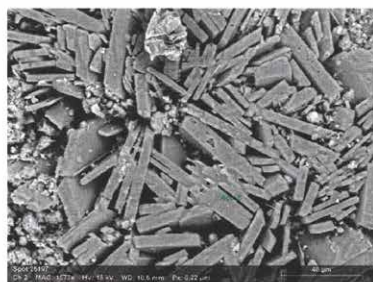
D. Crusts on passage floors

The gully stream above the cave's upper entrance does not flow into the cave under drought conditions and the only water remaining in the cave under those conditions is seen as isolated pools. Under these conditions, last observed in September 2020, a dry crust covers the passage floor (Fig. 17).

Although samples of the dry floor crust were not taken, to simulate the formation of this crust, 500 ml of cave water was gradually evaporated until a smooth hard residue remained (Fig. 18).

The composition of this crust as per powder XRD (Fig. 19) is a mix of 38% thenardite, 10% blodite, and 54% konyaite ($\text{Na}_2\text{Mg}(\text{SO}_4)_2 \cdot 5\text{H}_2\text{O}$) with a distinctive 2θ 7.5 degree peak on the diffractogram for the konyaite. Although thenardite and blodite were expected to be present, the presence of konyaite was not.

The hydrated double salt konyaite was first identified in 1984 (van



Name	Date	Time	HV [kV]	Mag	WD [mm]
Spot 26197	12/15/2021	11:59:31 AM	15.0 keV	1573x	10.6 mm

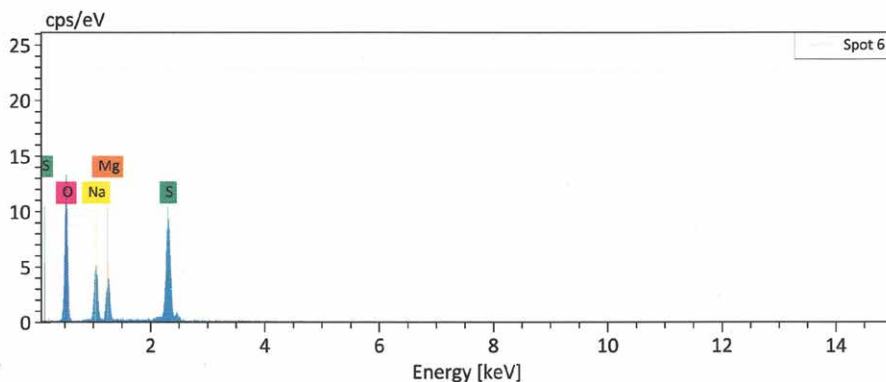


Figure 11. Tabular blodite with EDX spectrum.

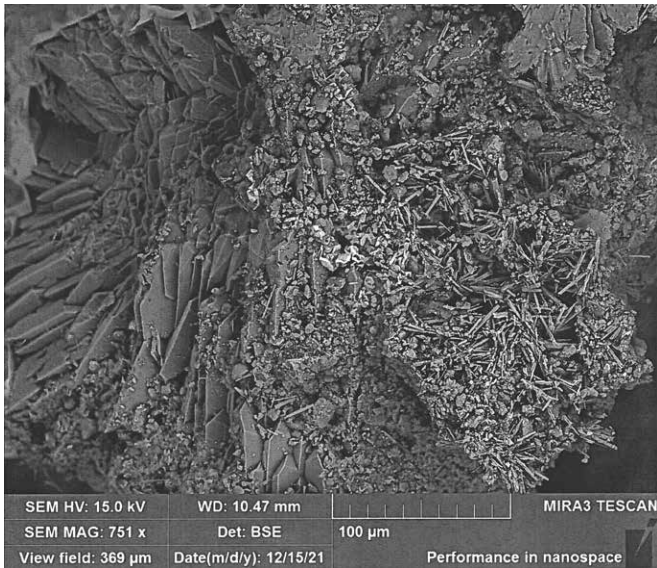


Figure 12. SEM image of bipyramidal thenardite (left) and needle thenardite (right).

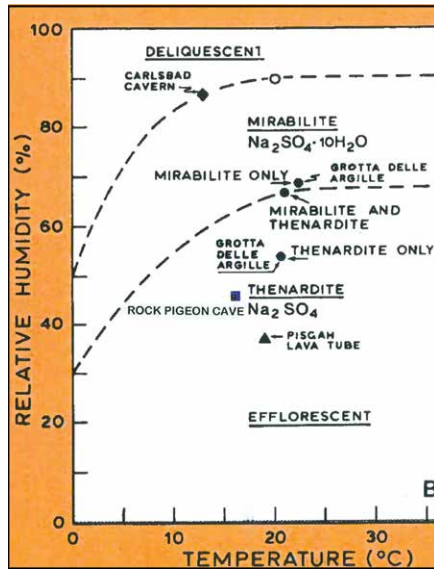


Figure 13. Stability of mirabilite and thenardite as a function of temperature and relative humidity (from Hill, C. and P. Forti, 1997, Fig. 179B).

Doesburg, J. et. al, 1982) and to date has only been documented in one other cave: Tausoare Cave in Romania (Onac, B.P., et. al., 2001). Whether konyaite will be present in crustal material in Rock Pigeon Cave, however, remains to be seen. Ambient conditions in the cave (17 °C, 45 % RH) differ from those in which the simulated crustal material was produced (20 °C, 25 % RH) and this may influence the crystallization of konyaite.



Figure 14. Subaqueous deposits (sulfates?) in cave pool.

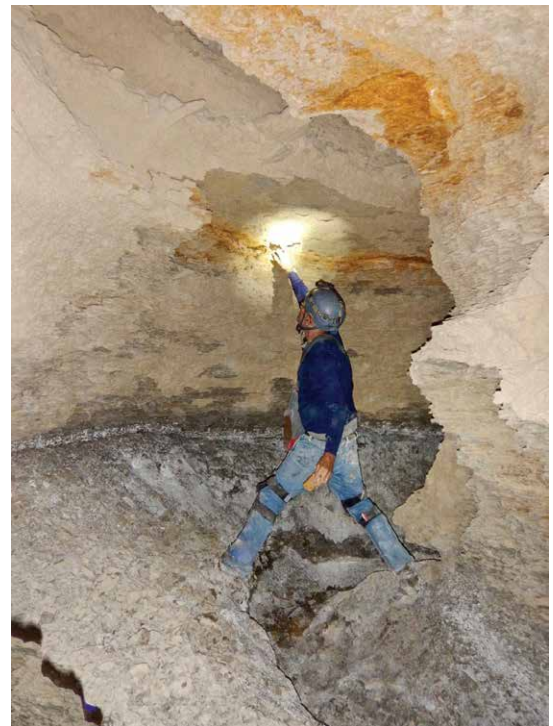


Figure 15. Sulfate coatings on damp shale slopes.



Figure 16. Sulfate coating on damp shale, 3cm diam.

E. Evaporites on passage walls

Needles, beards, and hair-like growths are observed on dry passage walls 1-2 m above the high water line in the cave (Fig. 20). These ephemeral minerals appear seasonally and are not the result of evaporation of sulfate-saturated water flowing through the cave.



Figure 17. Dry crust on passage floor.



Figure 18. Simulated crust from evaporated cave stream water.

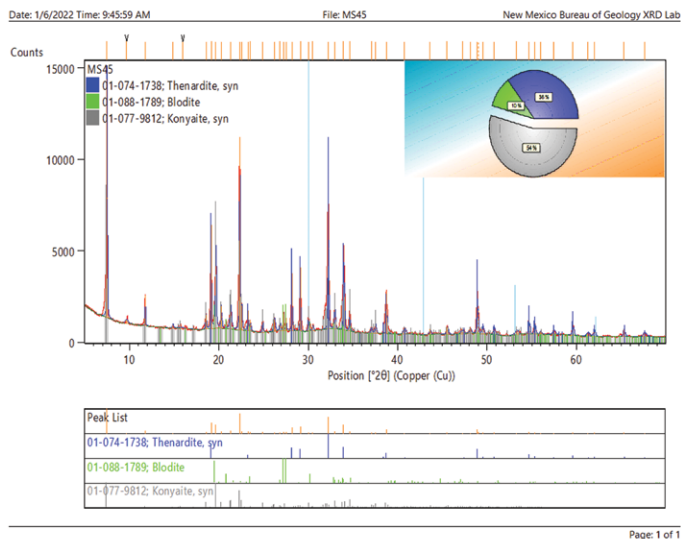


Figure 19. Diffractogram for crusted material derived from evaporated cave stream water.

In a sample taken (MS33), the composition of this material was 16 % gypsum, 20 % thenardite, 16 % blodite and 5 % carbonates (calcite and dolomite). The remaining material, probably derived from the shale wall, consisted of 9 % quartz and 34 % clays: kaolinite and illite.

The needles develop as a result of evaporation of salt-rich fluids at the rock/air interface, producing salt efflorescences (De Waele, J. et al., 2017). Precipitation-derived surface water within the shale reacts with pyrite to produce sulfate ions. These react with calcium ions derived from the carbonate component of the shale to produce gypsum.



Figure 20. Mixed sulfates on passage wall.

Pressure created by hydration of the gypsum results in the extrusion of the needles from the passage walls. Cations in the clays in the shale, particularly Na^+ and Mg^+ derived from illite and montmorillonite, combine with SO_4^{2-} from in situ pyrite oxidation to produce the thenardite and blodite components of the observed mixed-sulfate needles.

CONCLUSIONS

This paper provides a preliminary assessment of the development and mineralogy of a relatively large vadose cave in a Cretaceous shale. Conditions required for this type of cave to develop involve a semi-arid to arid climate, the presence of swelling soils (montmorillonite) that enhance the movement of surface water through the regolith, pyrite in the shale to create sulfate ions, and sufficient calcite in the shale to allow it to react with the sulfate ions. The resulting gypsum wedges apart the shale beds and increases secondary porosity, allowing shale particles to be removed from initial openings, thus enlarging these openings on a granular basis via water flowing to a lower outlet, i.e., corrosion. Because the combination of these conditions occurs infrequently, vadose caves are rarely found in shale bedrock.

Ions from soluble salts found in Mancos soils are carried into these caves by entering streams. Evaporation of these salt-containing fluids on clay and rock surfaces result in the precipitation of sodium sulfate salts such as thenardite, blodite, and hexahydrate. Gypsum is also precipitated and being less soluble than the sulfates, comes out of solution first. As pools in the caves evaporate and ion concentrations increase to a point where saturation indices become positive, these salts come out of solution, forming sulfate crusts on passage floors. The subaqueous precipitation of sulfates in cave pools is also observed, consistent with subaqueous crystallization seen in evaporating hypersaline lakes. Finally, following occasional precipitation events where meteoric water reaches the shale and reacts with minerals within, the slow evaporation of the resulting salt-rich water at the rock/air interface on passage walls results in efflorescences, primarily mixed-sulfate minerals.

ACKNOWLEDGEMENTS

The work described in this paper was carried out under a Research Agreement with the U.S. Bureau of Land Management office in Grand Junction, CO, administered by Dr. Madeline (Nikki) Grant-Hoffman. X-Ray diffraction analyses were conducted by the XRD laboratory at the New Mexico Bureau of Geology and Mineral Resources in Socorro, NM. Laboratory Manager Kelsey McNamara provided valuable insights in interpreting the results obtained. Scanning electron microscopy and energy dispersive spectroscopy of shale and mineral samples was carried out at the Colorado School of Mines with Prof. John Spear and also with Prof. Katharina Pfaff at the CSM Automated Mineralogy Laboratory. Richard Heemskerk at the Environmental Isotope Laboratory, University of Waterloo, Ontario did the stable sulfur isotope analysis of the gypsum samples collected in caves. Valuable review comments on earlier drafts of this paper were made by Dr. Carleton Bern at the USGS Colorado Water Science Center in Lakewood, CO. Dr. Bern also carried out the simulation of cave water evaporation using PHREEQC. Ed LaRock provided field support and made insightful observations about structural geology and geologic setting both in the area and in the cave. Finally, photographic documentation of features in the cave and in survey and cartography were conducted by Bob Richards and Carol Vesely.

REFERENCES

- Cabestrero, O., P. del Buey and M. Esther Sanz-Montero, 2018, Biosedimentary and geochemical constraints on the precipitation of mineral crusts in shallow sulphate lakes: *Sedimentary Geology* v. 366, p. 32-46.
- Cline, A.J., C. Spears, F. Mehaffey, et. al., 1967, Soil Survey Delta-Montrose Area, Colorado: U.S. Department of Agriculture Soil Conservation Service, 73 p.
- De Waele, J., C. Carbone, L. Sanna, M. Vattano, E. Galli, F. Sauro and P. Forti, 2017, Secondary Minerals from Salt Caves in the Actama Desert (Chile): a hyperarid and hypersaline environment with potential analogies to the Martian subsurface: *International Journal of Speleology*: v. 46, p. 51-66.
- del Buey, P., M. Esther Sanz-Montero, O. Braissant, O. Cabestrero, and P.T. Visscher, 2021, The role of microbial extracellular polymeric substances on formation of sulfate minerals and fibrous Mg-clays: *Chemical Geology* v. 581, p. 1-16. <https://doi.org/10.1016/j.chemgeo.2021.120403>
- Elliott J. G., J.R. Herring, G.P. Ingersoll, J. Kosovich, and J. Fahy, 2007, Rainfall-Runoff and Erosion Data from the Mancos Shale Formation in the Gunnison Gorge National Conservation Area, Southwestern Colorado, 2003-2006: U.S. Geological Survey Open-File Report 2007-1002G, 68 p.
- Evangelou, V. P., L. D. Whittig, and K. K. Tanji, 1984, Dissolved Mineral Salts Derived from Mancos Shale: *Journal of Environmental Quality*, v.13, issue 1, p.146-150.
- Gu X, D. Rempe, W. Dietrich, A. Joshua West, T-C Lin, L. Jin, and S. Brantley, 2020, Chemical reactions, porosity, and microfracturing in shale during weathering: The effect of erosion rate: *Geochimica et Cosmochimica Acta*, v. 269, p. 63-100.
- Hansen, W.R., 1971, Geologic Map of the Black Canyon of the Gunnison River and Vicinity, Western Colorado, U.S. Geological Survey Miscellaneous Geologic Investigations Map I-584, 2 sheets, scale 1:31,680.
- Hill, C. and P. Forti, 1997, *Cave Minerals of the World*, 2nd Edition: Huntsville, Alabama, National Speleological Society, 463 p.
- Kellogg, K., W. Hansen, K. Tucker, and D. Paco Van Sistine, 2004, Geologic Map Gunnison Gorge National Conservation Area, Delta and Montrose Counties, Colorado, U.S. Geological Survey Scientific Investigations Map 2825, scale 1:45 000, 1 sheet.
- Miller, R.O., R. Gavlak, and D. Horneck, 2013, Soil, Plant and Water Reference Methods for the Western Region, Western Coordinating Committee on Nutrient Management, WERA-103.

- Medville, D., 2018, Speleogenesis of Caves in a Cretaceous Shale: Bighorn Basin, Wyoming: *Journal of Cave and Karst Studies*, v. 80, p. 66-80.
- Mees, F., C. Castaneda, J. Herrero, E. Van Ranst, 2011, Bloedite sedimentation in a seasonally dry saline lake (Salada Mediana, Spain): *Sedimentary Geology* v. 238 issues 1-2, p. 106-115.
- Merkler, D., N. McMillan, and B. Buck, 2006, Salt Mineralogy of Las Vegas Wash, Nevada: Morphology and Subsurface Evaporation: *Soil Science Society of America Journal*, v. 70, p. 1639-1651.
- Noe, D.C., J. L. White, and M. Nelson, 2015, Geologic Map of the North Delta quadrangle, Delta County, Colorado: Colorado Geological Survey Open File Report 15-09, scale 1: 24 000, 1 sheet, 9 p. text.
- Noe, D.C., M.L. Morgan, P.R. Hanson, and S. M. Keller, 2007, Geologic Map of the Montrose East Quadrangle, Montrose County, Colorado: Colorado Geological Survey Open-File Report 07-02, scale 1: 24 000, 2 sheets, 101p.
- Nordstrom, D.K., 1982, Aqueous Pyrite Oxidation and the Consequent Formation of Secondary Iron Minerals. Chapter 3 in Kittrick, A., D.S. Fanning, and L.R. Hossner, eds., *Acid Sulfate Weathering*, v. 10, Soil Science Society of America, p. 56-77
- Onac, B. P., W. B. White, and I. Viehmann, 2001, Leonite $[K_2Mg(SO_4)_2 \cdot 4H_2O]$, konyaite $[Na_2Mg(SO_4)_2 \cdot 5H_2O]$ and syngenite $[K_2Ca(SO_4)_2 \cdot H_2O]$ from Tausoare Cave, Rodnei Mts., Romania. *Mineralogical Magazine*, February 2001, v. 65(1), p. 103-109.
- Onac, B. P. and P. Forti, 2011, Minerogenetic mechanisms occurring in the cave environment: an overview: *International Journal of Speleology*, v. 40, p. 79-98.
- Palmer, A., 2007, *Cave Geology*: Dayton, Ohio, Cave Books, 454p.
- Parkhurst, D.L. and C.A.J. Appelo, 1999, User's Guide to PHREEQC (version 2); A Computer Program for Speciation, Batch-Reaction, One-Dimensional Transport, and Inverse Geochemical Calculations: U.S. Geological Survey Water Resources Investigation Report 99-4259, 312p.
- Penner, E., W.J. Eden, and P.E. Grattan-Bellew, 1972, Expansion of Pyritic Shales: Canadian Building Digest, Division of Building Research, National Research Council Canada, 6p.
- Sonmez, I., 2010, Actual Bloedite mineral Precipitation in a Seasonal Lake in Cankiri-Corum Basin: *Bulletin of the Mineral Research and Exploration*, v. 140, p. 35-53.
- Sonnenfeld, P., 2003, Evaporites, in R. A. Meyers, ed., *Encyclopedia of Physical Science and Technology* (third edition): San Diego, California, Academic Press, p. 653-671.
- Tuttle, M.L., J. Fahy, J. Elliott, R. Grauch and L. Stillings, 2014, Contaminants from Cretaceous black shale I. Natural weathering processes controlling contaminant cycling on Mancos Shale, southwestern United States, with emphasis on salinity and selenium: *Applied Geochemistry* v. 46. p. 57-71. <https://doi.org/10.1016/j.apgeochem.2013.12.010>
- U.S. Department of Agriculture, 2018, Final Watershed Plan and Environmental Assessment for the Lower Gunnison Project: Figure 3.2-1.
- U.S. Department of Energy, 2011, Natural Contamination from the Mancos Shale: Report ESL-RPT-2011-1, 78 p.
- van Doesburg, J., L. Vergouwen, van der Plas, L., 1982. Konyaite, $Na_2Mg(SO_4)_2 \cdot 5H_2O$, a new mineral from the Great Konya Basin, Turkey: *American Mineralogist*, v. 67, p. 1035-1038.
- White, J.L., R. MacLean and C.J. Carroll, 2014, Geologic Map of the Whitewater Quadrangle Mesa County, Colorado, Colorado Geological Survey Open File Report 14-09, scale 1:24 000, 2 sheets, 42 p text.
- White, J.L. and C. Greenman, 2008, Collapsible Soils in Colorado: Denver, Colorado, Colorado Geologic Survey Publication EG-14, 108 p.
- Whittig, L. D., A. E. Deyo and K. K. Tanji, 1982, Evaporite mineral species in Mancos Shale and Salt Efflorescence, Upper Colorado River Basin: *Soil Science of America Journal*, v. 46, issue 3, p. 645-651.